Electronic Supplementary Material (ESI) for Catalysis Science & Technology.

Facet-engineering palladium nanocrystals for remarkable photocatalytic dechlorination of polychlorinated biphenyls

Wei Guo, Binbin Guo, Huiling Chen, Cheng Liu and

Ling Wu*

State Key Laboratory of Photocatalysis on Energy and Environment, Fuzhou University, Fuzhou, 350116, China.

* E-mail address: wuling@fzu.edu.cn

1. Experimental section

1.1. Materials

Sodium tetrachloropalladate (Na_2PdCl_4), 2,2′,6,6′-tetramethylpiperidine *N*-oxyl (TEMPO) and 3,3′,4,4′-trtrachlorobiphenyl (PCB77) were purchased from Shanghai Aladdin Bio-Chem Technology Co., Ltd. Polyvinylpyrrolidone (PVP; Mw: ~55000), KBr, ascorbic acid, citric acid, acetone, ethylene glycol (EG), Titanium tetrachloride ($TiCl_4$), methanol, ethanol and N, N-dimethylformamide (DMF) were all obtained from Sinopharm Chemical Reagent Co., Ltd (Shanghai, China). Water used in all experiments was ultrapure. All chemicals were used as received without further purification.

1.2. Preparation of TiO_2(B) nanosheets

TiO_2(B) nanosheets were synthesized by our previously reported method.[1] Typically, 2 mL $TiCl_4$ and 70 ml of EG were mixed. Then 2 mL of water was introduced into the mixture. The resulting light-yellow solution was transferred into a 100 mL Teflon-lined steel autoclave, and then was kept at 150 ℃ for 6 h. After being cooled to room temperature, the white powder was separated by centrifugation and washed with ethanol and deionized water several times.

1.3. Synthesis of Pd nanocrystals

Synthesis of Pd cube (CUB ~8 nm), 57 mg of K_2PdCl_4 was thoroughly dissolved in 3 ml of ultrapure water by extensively mixing for 1h. 105 mg of PVP, 300 mg of KBr, and 60 mg of ascorbic acid were dissolved in 8 ml of ultrapure water. [2-3] The PVP-KBr-ascorbic acid solution was pre-heated in an oil bath at 80 °C for 5 min, and then

K_2PdCl_4 solution was added quickly. The reaction solution was kept stirring at 520 rpm and maintained at 80 °C in air for 3 h, and the solution was collected after naturally cooling down. An excess amount of acetone was used to precipitate the nanoparticles. The product was collected by centrifugation and washed with ethanol/water several times to remove excess PVP. Finally, Pd cube NCs were stored in aqueous stock suspensions.

Synthesis of Pd octahedron (OCT ~ 8 nm), 5 mL of ethylene glycol was preheated in a reaction vial at 110 °C for 1 h. 184.5 mg of K_2PdCl_4 was thoroughly dissolved in 4 mL of ethylene glycol by extensive mixing for at 1 h, and 106.7 mg of PVP was dissolved in 4 mL of ethylene glycol.[4-5] 3 mL of each K_2PdCl_4 solution and PVP solution was injected simultaneously into the reaction vial at a flow rate of 5 mL h^{-1}. The mixed solution was stirred at 520 rpm and maintained at 110 °C in air for 3 h, and the solution was collected after naturally cooling down. An excess amount of acetone was used to precipitate the nanoparticles. The product was collected by centrifugation and washed with ethanol/water several times to remove excess PVP. Finally, Pd octahedron NCs were stored in aqueous stock suspensions.

Preparations of Pd nanocrystals/TiO_2(B) nanosheets (CUB/TBs, OCT/TBs), The CUB and OCT have been anchored onto TiO_2(B) nanosheets (TBs) by a wet-chemical impregnation method.[6] TiO_2(B) nanosheets were dispersed into the water solution of as-synthesized Pd NCs (CUB and OCT). The mixed solution was sonicated for 2 h. The catalysts were collected by centrifugation, labeling as untreated CUB/TBs and untreated OCT/TBs, respectively. The samples, are labeled CUB/TBs and

OCT/TBs, respectively, washed with ethanol and ultrapure water several times to remove excess PVP. Finally, all products were processed by photoreduction process to generate surface defects.

1.4. Characterization

Powder X-ray diffraction (XRD) tests were carried out on a Bruker D8 Advance X-ray diffractometer (Cu $K\alpha_1$ radiation, λ = 1.5406 Å). Transmission electron microscopy (TEM) studies were performed on a FEI Talos field emission transmission electron microscope at an accelerating voltage of 200 kV. X-ray photoelectron spectroscopy (XPS) data were taken on a PHI Quantum 2000 XPS system with a monochromatic Al Kα source and a charge neutralizer. The binding energy of reference C 1s is 284.8 eV. UV-vis diffuse reflectance spectra (UV-vis DRS) were obtained by using a UV-vis spectrophotometer (Varian Cary 500) and the data were converted to Kubelka-Munk (KM) functions. $BaSO_4$ was used as the reflectance standard. The Brunauer-Emmett-Teller (BET) surface area determination was measured on Micromeritics 3500 M apparatus. These samples were degassed at 120 °C for 6 h, the nitrogen adsorption and desorption isotherms were measured at -196 °C. The Fourier transform infrared (FT-IR) spectra of the prepared samples was carried out on a Nicolet IS50 Fourier transform infrared spectrometer at a resolution of 4 cm^{-1}. The content of Pd nanoparticles in aqueous stock suspensions were examined by Inductively Coupled Plasma (ICP) using PerkinElmer (Avio 200). The room temperature photoluminescence (PL) characterizations were carried out on an Edinburgh FI/FSTCSPC 920 spectrophotometer. Electron spin resonance (EPR) spectra were recorded by a Bruker

A300 spectrometer at room temperature. An Epsilon Electrochemical System was used to perform the electrochemical analysis in a three-electrode cell (counter electrode, Pt plate; reference electrode, Ag/AgCl). Fluorine-tin oxide (FTO) glass was used as the conductive substrate to prepare the working electrode. Typically, the sample (5 mg) was totally dispersed in DMF (1 mL) by sonication to gain a slurry. Afterward, the resultant slurry was spread onto the FTO glass. The transient photocurrent response spectra were collected in Na_2SO_4 aqueous solution (0.2 M) with a 300 W Xe lamp ($\lambda \geq$ 400 nm) as a light source, and the applied bias potential was -0.4 V vs Ag/AgCl (Ph = 6.8). A 300 W Xe lamp (PLS-SXE 300, Beijing Perfectlight Co. Ltd) was used as a light source.

1.5. In-situ FTIR measurement

The in-situ FTIR spectra of CO adsorbed on CUB/TBs and OCT/TBs were carried out on a Nicolet IS50 Fourier transform infrared (FT-IR) spectrometer. A total of 64 scans at a resolution of 4 cm^{-1} were performed to obtain each spectrum. Firstly, a powder sample (10 mg) was pressed into a self-supporting IR disk. The disk was then put into the sample holder which could be moved vertically along the cell's tube. Before measurements, the disk was treated under dynamic vacuum (4×10^{-2} hPa) at 150 °C for 2 h to remove surface contaminants. After the disk cooling to room temperature, the FTIR spectrum of a sample was collected. Then, 1 mL of CO was spiked into the cell with a syringe via a septum. After adsorption equilibrium was reached for 1 h, another FTIR spectrum was taken for revealing the information of CO on CUB/TBs and OCT/TBs, respectively.

1.6. Photocatalytic dechlorination of PCB77

PCB77 stock solution (1×10^{-3} mol/L) in methanol was diluted with methanol-water mixture (methanol: water = 70: 30) to 2×10^{-5} mol/L. In a typical run, 8 mg of a catalyst was added to 2 mL of PCB77 solution. The suspension was ultrasonically mixed for 1 min and purged with argon for 30 min to remove O_2 in the dark. To eliminate the ultraviolet, a cut-off filter was used to cut off the irradiation below 400 nm. The reaction at different times were carried out separated. After irradiated a given time, the suspensions were centrifuged at 8000 rpm for 2 min and the supernatants were filtered through a 0.22 μm membrane. The filtrates were used for HPLC (Agilent Technologies 1260 Infinity) analysis. The dechlorination efficiency for PCB77 is calculated according to the following equation:

Dechlorination efficiency (%) =

$$\frac{C(PCB35 + PCB37) \times 1 + C(PCB11 + PCB13) \times 2 + C(PCB2 + PCB3) \times 3 + C(DE)\ \times 4}{C_0(PCB77) \times 4} \times 100\%$$

2. Theoretical section

All spin-polarized DFT calculations were performed using the Vienna ab initio Simulation Packages (VASP).[7-9] Based on experimental observations, for the Pt models with 36 atoms, the dominant (100) and (111) crystal facets was exposed and the 2 upper atomic layers were relaxed and a 20 Å-thick vacuum layer was introduced to prevent mutual influence between the two adjacent slabs. The projected-augmented wave (PAW) pseudopotentials were utilized to describe the core electrons and the cut-off energy was set to be 450 eV.[10] A plane-wave kinetic energy cutoff of 400 eV was used

to treat the valence electrons. The exchange-correlation potential was treated by the Perdew−Burke−Ernzerhof (PBE) version of the generalized gradient approximation (GGA).[11] All the structures were relaxed until the forces on each ion were less than 0.02 eV/Å, and the convergence criteria for the energy was set as 10^{-5} eV. The Brillouin's zone integration was performed on 4× 4×2 kpoints of gamma centre for all the models. The model construction and data processing are assisted by the VASPKIT [12] and QVASP [13] softwares.

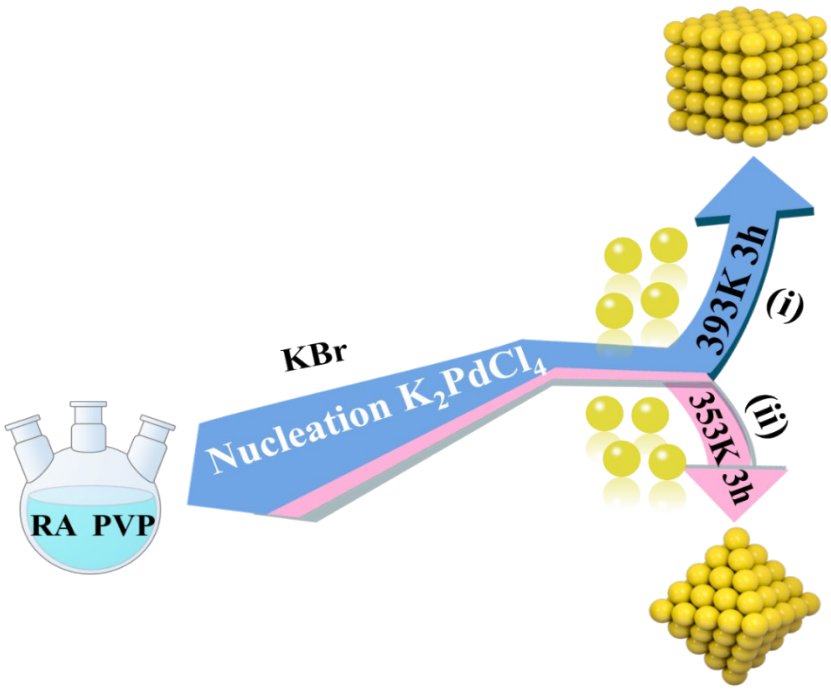

Fig. S1 Overall flowchart for the fabrication of CUB (a) and OCT (b).

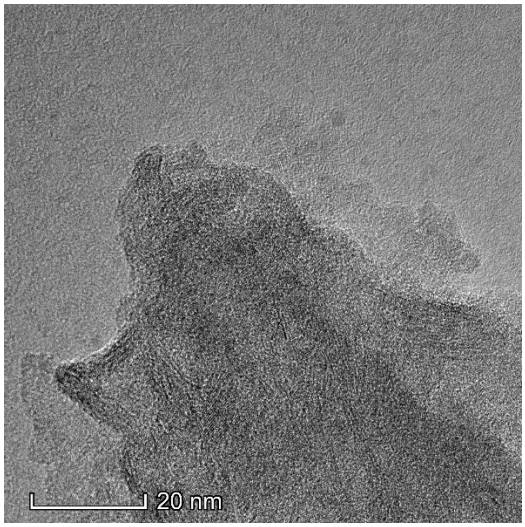

Fig. S2 TEM image of TBs.

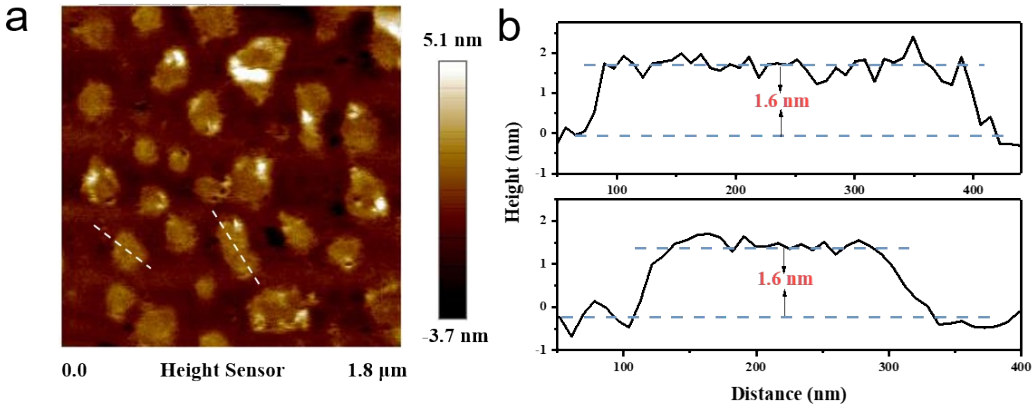

Fig. S3 AFM (a) and the corresponding height images (b) of TBs.

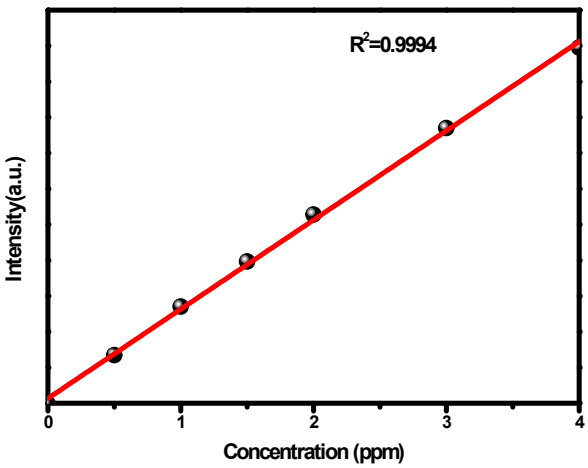

Fig. S4 Standard curves for Pd (ppm=mg L^{-1}).

Table S1. Pd NPs concentration of CUB/TBs and OCT/TBs.

	CUB/TBs	OCT/TBs
Pd concentration (ppm)	1.064	0.954

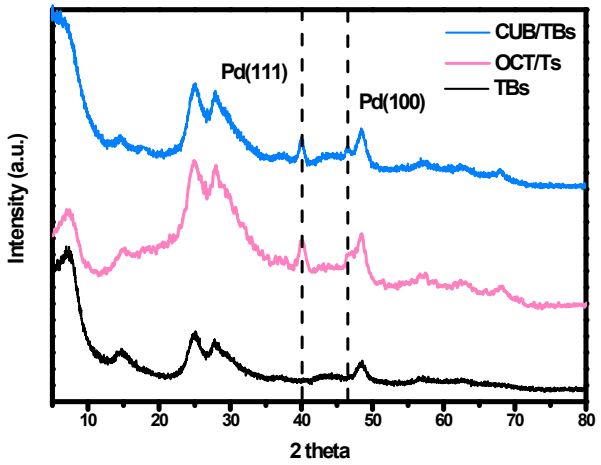

Fig. S5 XRD patterns of TBs, OCT/TBs and CUB/TBs.

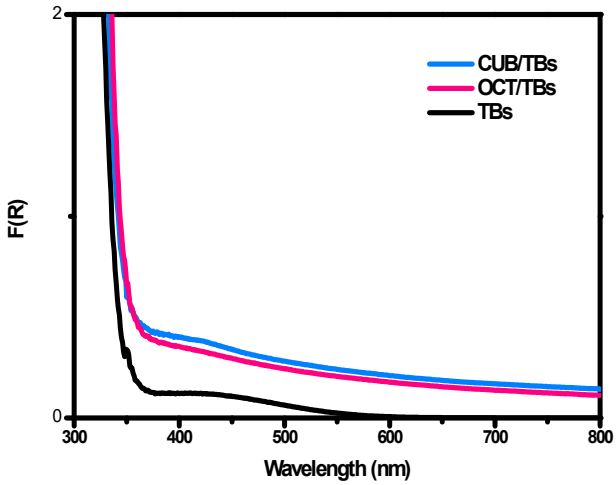

Fig. S6. DRS spectra of TBs, OCT/TBs and CUB/TBs.

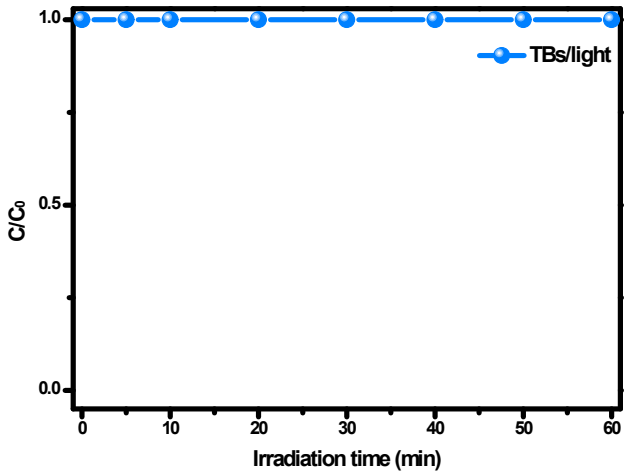

Fig. S7 Temporal concentration changes (C/C_0) of PCB77 over TBs under visible light.

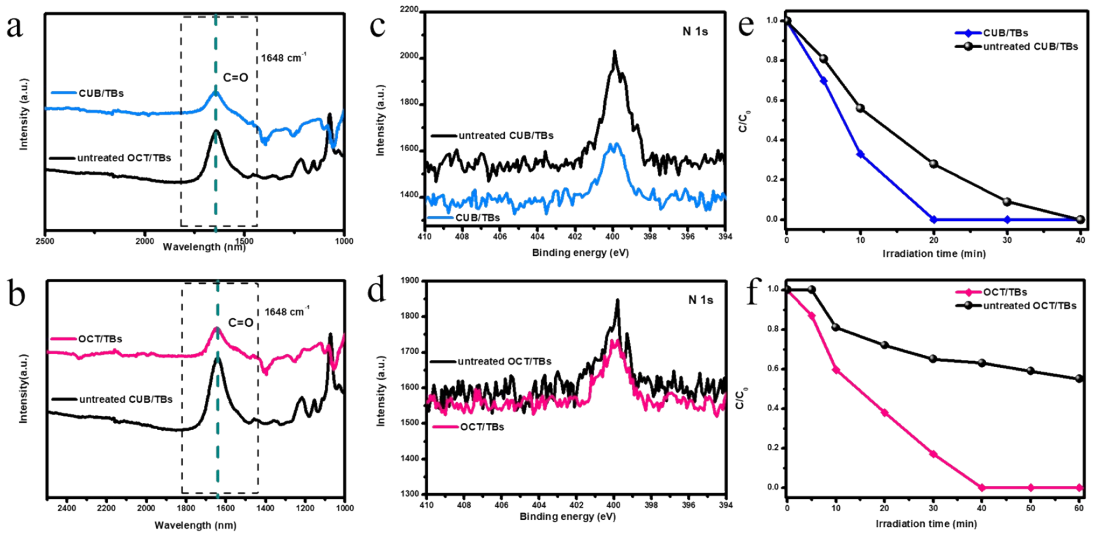

Fig. S8 FTIR spectra (a), XPS spectrum of N 1s (c), Temporal concentration changes (e) of PCB77 for CUB/TBs and untreated CUB/TBs; FTIR spectra (b), XPS spectrum of N 1s (d), Temporal concentration changes (d) of PCB77 for OCT/TBs and untreated OCT/TBs.

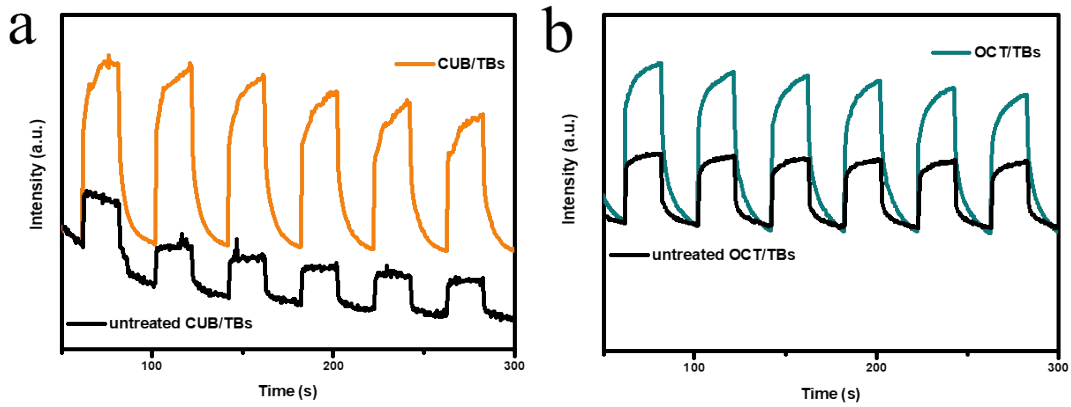

Fig. S9 Photocurrent response of CUB/TBs and untreated CUB/TBs(a); OCT/TBs and untreated OCT/TBs (b).

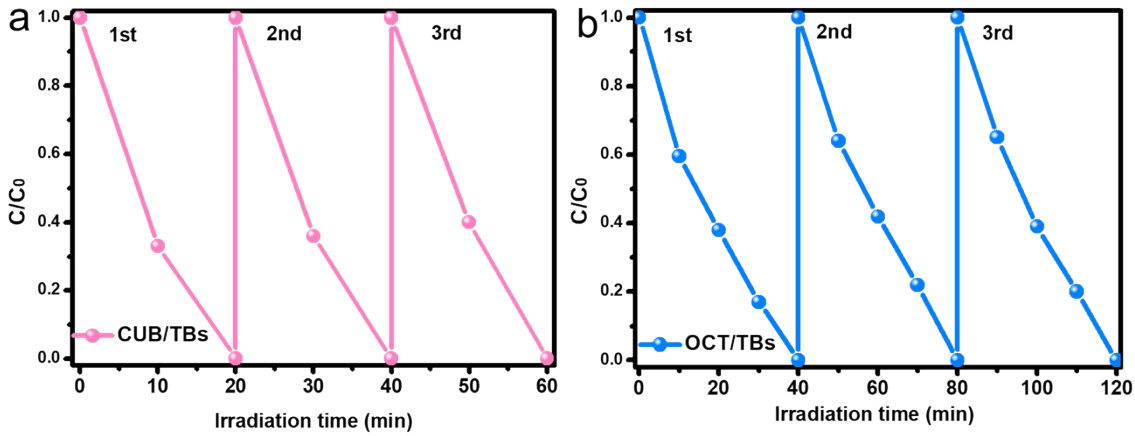

Fig. S10 Temporal concentration changes of PCB77 three times for CUB/TBs (a) and OCT/TBs (b).

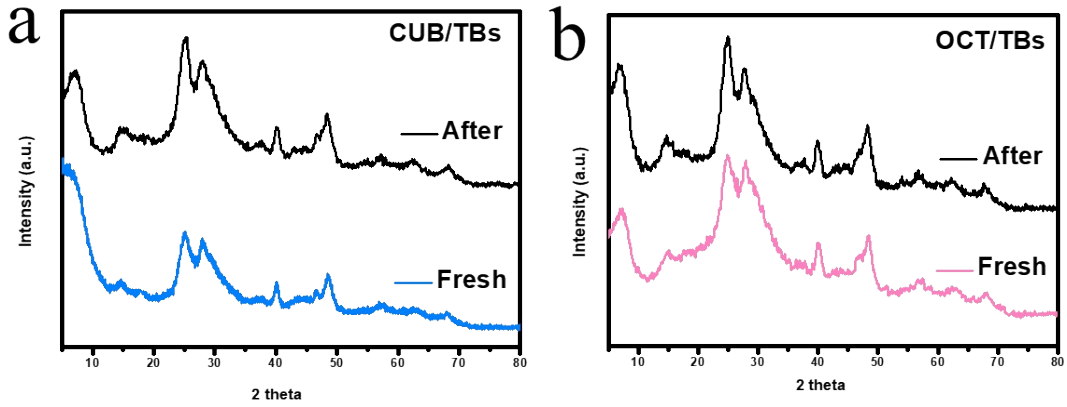

Fig. S11. XRD patterns of CUB/TBs before and after three photocatalytic reaction (a),

OCT/TBs before and after three photocatalytic reactions (b).

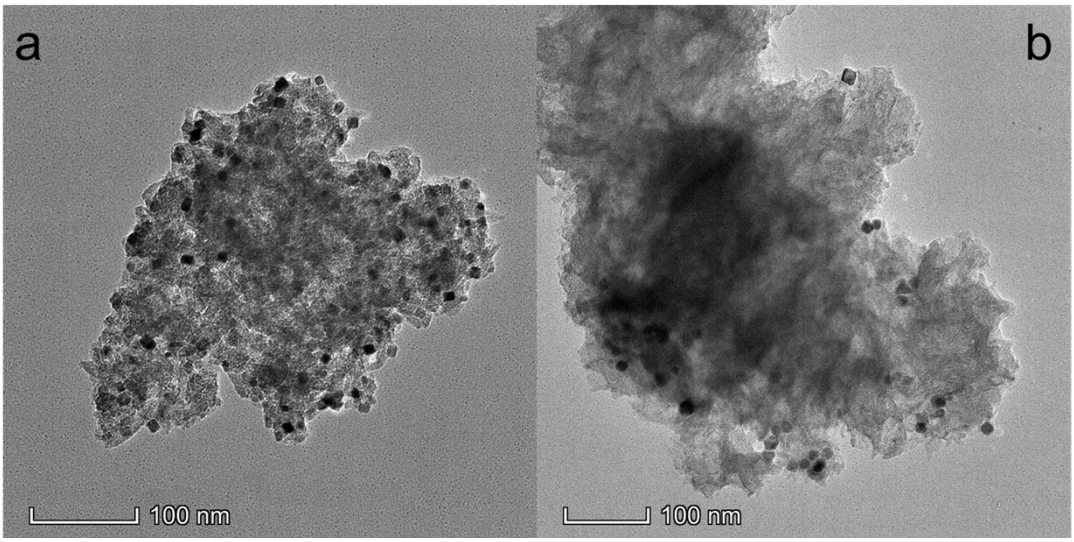

Fig. S12 TEM image of CUB/TBs and OCT/TBs after three photocatalytic reactions.

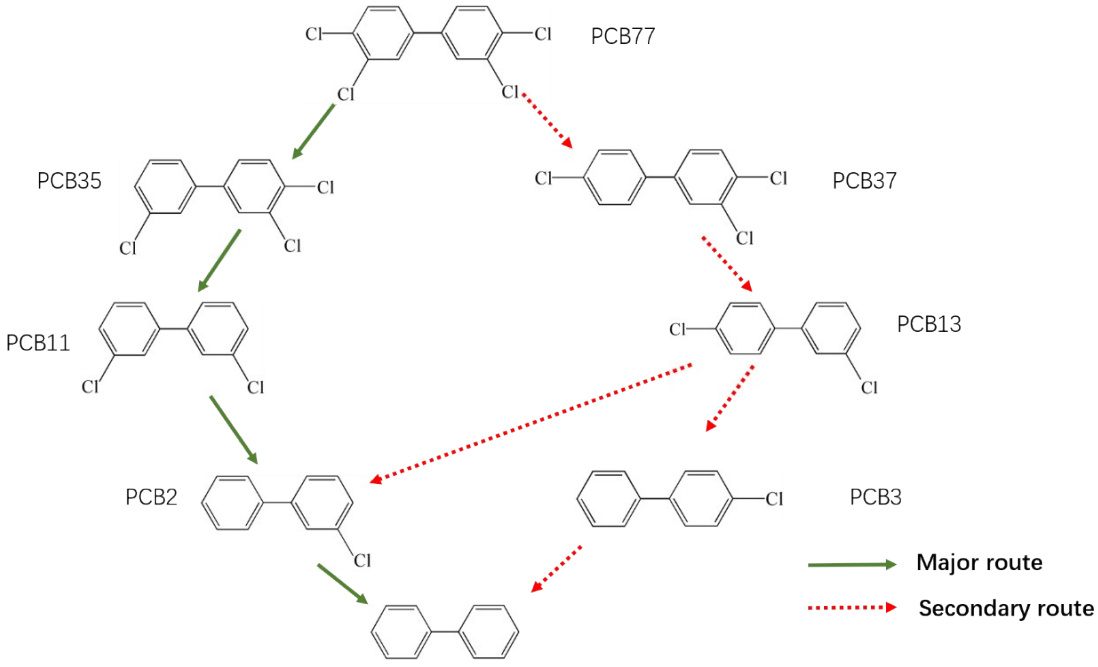

Fig. S13 Pathways of the photocatalytic dechlorination of PCB77.

Table S2. TON and TOF value of biphenyl on CUB/TBs and OCT/TBs.

	TON[a]	**TOF[b]**
CUB/TBs	0.053	0.085/h
OCT/TBs	0.036	0.054/h

[a] Moles of biphenyl produced per mole of Pd,

[b] Moles of biphenyl peoduced per mole of Pd per hour.

Table S3. Performance comparison of various photocatalysts for photocatalytic dehalogenation for halogenated compounds.

Light source	Photocatalyst	Substrate	Reaction time(min)	Reference
λ≥400 nm (300W Xe lamp)	CUB/TB (8mg)	PCB77 (20μmol/L) 2mL	20	This work
	OCT/TB (8mg)	PCB77 (20μmol/L) 2 mL	40	
λ≥400 nm (300W Xe lamp)	0.75%Pd/TiO_2(B) (8mg)	PCB77(20μmol/L) 2 mL	100	[14]
	0.75%Pd/C_3N_4 (8mg)	PCB77 (20μmol/L) 2 mL	>120	
Mercury-vapor lamp 450 W medium pressure	Pd/Cu_2O (100mg)	PCB77 (25μmol/L) 50 mL	9600	[15]
	Pd/Cu_2O (100mg)	PCB2 (25μmol/L) 50 mL	900	
Mercury lamp 450 W medium pressure	0.5%Pd/TiO_2 （5mg）	BDE209 (10μmol/L) 25 mL	60	[16]

BDE209: decabromodiphenyl ether

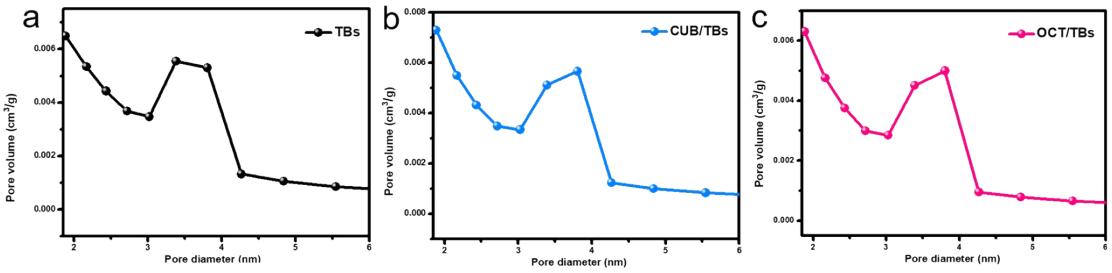

Fig. S14 Pore size distribution of TBs, CUB/TBs and OCT/TBs.

Table S4. Summary of surface area and pore volume of TBs, OCT/TBs and CUB/TBs.

Samples	BET surface areas (m^2/g)	Pore volume (cm^3/g)
TBs	347.9	3.6
OCT/TBs	369.6	3.6
CUB/TBs	420.0	3.6

Table S5. Statistics of surface atoms and edge atoms for CUB and OCT.

	D	N_S/N_T	X_{100}	X_{111}	X_{edge}
CUB	8	12.7%	79.9%	-	12.4%
OCT	8	13.8%	-	74.2%	18.9%

D: the length of side for CUB and OCT

N_T: the total number of atoms

N_S: the number of surface atoms

N_i: the surface atoms of a given type

$X_i=N_i/N_S$

Table S6. FT-IR wavenumber and adsorption energy of CO adsorbed on CUB and OCT by different adsorption models.

Adsorption models	Wavenumber/cm^{-1}	Adsorption energy/eV
CUB bridge	1826.9	-2.265
CUB linear	2004.6	-2.485
OCT bridge	1777.1	-2.128
OCT linear	2020.9	-2.505

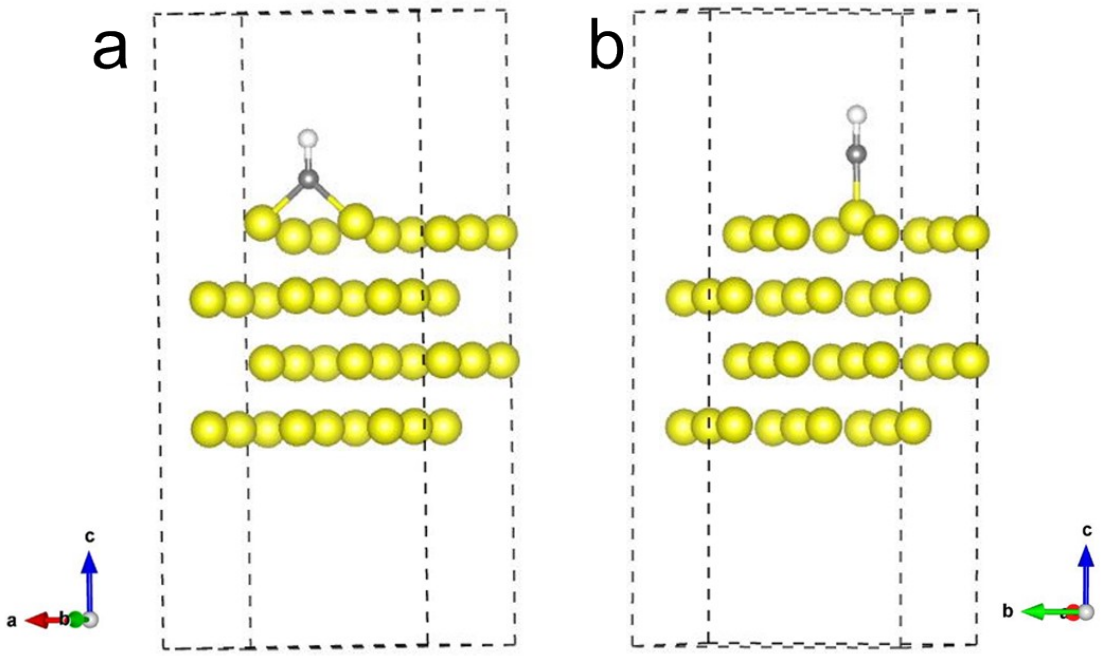

Fig. S15 CO absorption models on CUB by bridge (a) and liner (b).

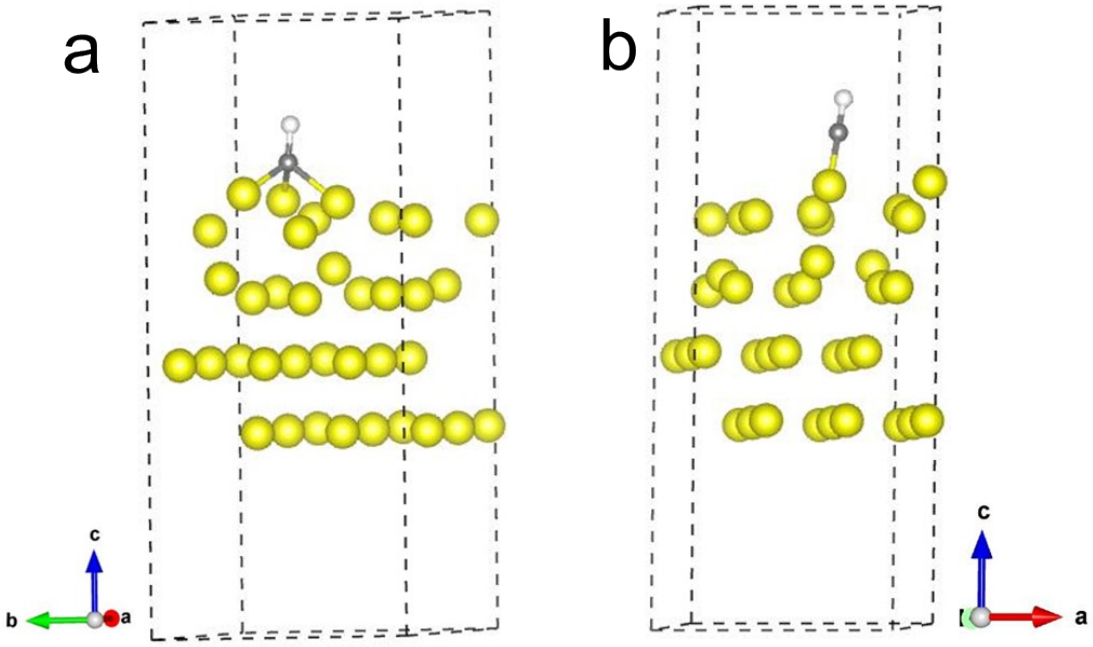

Fig. S16 CO absorption models on OCT by bridge (a) and liner (b).

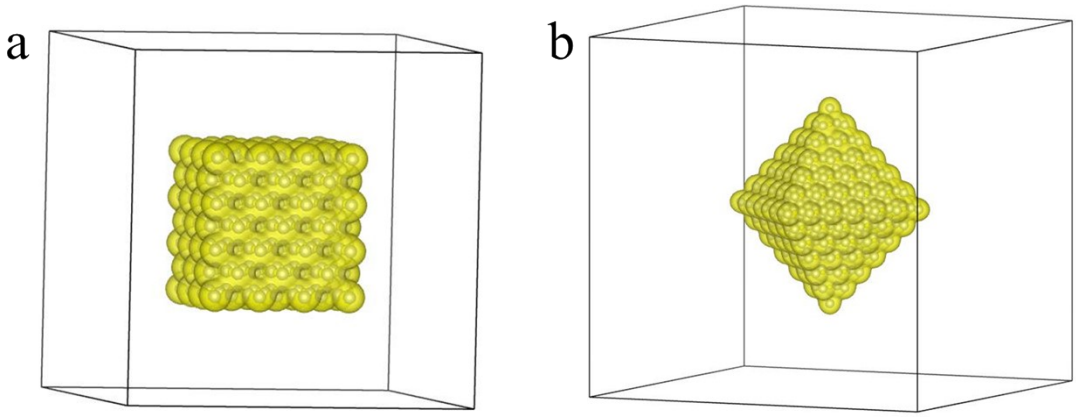

Fig. S17. Computed charge density (surface electrostatic potential) spatial distributions for Pd (100) (a) and (111) (b), where the isosurface level value is 0.02 e/A^3.

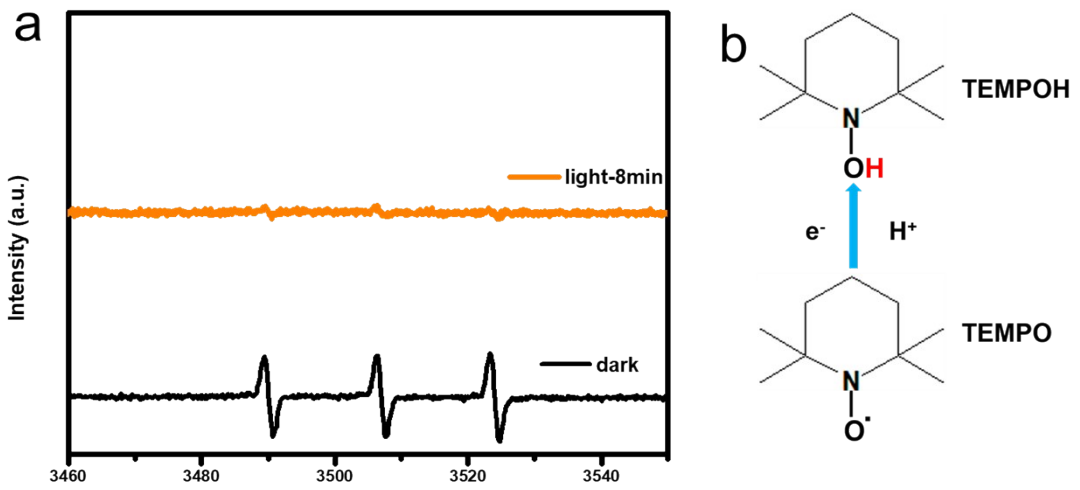

Fig. S18 EPR signals of TEMPO for CUB/TBs (a), The process of TEMPO to TEMPOH (b).

References

(1) W. Guo.; J. Zou.; B. Guo.; J. Xiong.; C. Liu.; Z. Xie.; L. Wu. Pd nanoclusters/TiO_2(B) nanosheets with surface defects toward rapid photocatalytic dehalogenation of polyhalogenated biphenyls under visible. Appl. Catal. B: Environ. **2020**, *277*, 119255.

(2) Shuai, D. M.; McCalman, D. C.; Choe, J. K.; Shapley, J. R.; Schneider, W. F.; Werth, C. J.; Structure Sensitivity Study of Waterborne Contaminant Hydrogenation Using Shape-and Size-Controlled Pd Nanoparticles. *ACS Catal*. **2003**, *3*, 453-463.

(3) Xiong, Y. J.; Chen, J. Y.; Wiley, B. J. M.; Xia, Y. N.; Understanding the Role of Oxidative Etching in the Polyol Synthesis of Pd Nanoparticles with Uniform Shape and Size. *J. Am. Chem. Soc.* **2005**, *127*, 7332-7333.

(4) Xiong, Y. J.; Cai, H. G.; Wiley, B. J. M.; Wang, J. G.; Kim, M. J.; Xia, Y. N.; Synthesis and Mechanistic Study of Palladium Nanobar and Nanorods. *J. Am.*

Chem. Soc. **2007**, *129*, 3665-3675.

(5) Lim, B. B.; Jiang, M. J.; Tao, J.; Camargo, P. H. C.; Zhu, Y. M.; Xia, Y. N.; Shape-Controlled Synthesis of Pd Nanocrystals in Aqueous Solutions. *Adv. Funct. Mater*. **2009**, *19*, 189-200.

(6) Xu, Z. N.; Sun, J.; Lin, C. S.; Jiang, X. M.; Chen, Q. S.; Peng, S. Y.; Wang, M. S.; Guo, G. C.; High-Performance and Long-Lived Pd Nanocatalyst Directed by Shape Effect for CO Oxidative Coupling to Dimethyl Oxalate. *ACS Catal*. **2013**, *3*, 118-122.

(7) Kresse, G.; Furthmüller, J.; Efficiency of ab-initio total energy calculations for metals and semiconductors using a plane-wave basis set, Comp. Mater. Sci. **1996**, *6*, 15-50.

(8) Kresse, G.; Furthmüller, J.; Efficient iterative schemes for ab initio total-energy calculations using a plane-wave basis set, Phys. Rev. B: Condens. Matter. **1996**, *54*, 11169-11186.

(9) Kresse, G.; Hafner, J.; Ab initio molecular-dynamics simulation of the liquid-metal--amorphous-semiconductor transition in germanium, Phys. Rev. B: Condens. Matter. **1994**, *49*, 14251-14269.

(10) Kresse, G.; Joubert, D.; From ultrasoft pseudopotentials to the projector augmented-wave method, Phys. Rev. B: Condens. Matter. **1999**, *59*, 1758.

(11) Perdew, J. P.; Burke, K.; Ernzerhof, M, Generalized Gradient Approximation Made Simple, Phys. Rev. Lett. **1996**, *77*, 3865-3868.

(12) V. Wang, N. Xu, J. C. Liu, G. Tang, W. T. Geng, VASPKIT: a user-friendly interface facilitating high-throughput computing and analysis using VASP code, Comput. Phys. Commun. **2021**, 267, 108033.

(13) W. Yi, G. Tang, X. Chen, B. Yang, X. Liu, qvasp: a flexible toolkit for VASP users in materials simulations, Comput. Phys. Commun. **2020**, 257, 107535.

(14) Guo, W.; Qin, Y.; Liu, C.; Guo, B. B.; Zou, J. H.; Xie, Z. H.; Wu, L.; Unveiling the intermediates/pathways towards photocatalytic dechlorination of 3,3′,4,4′-trtrachlorobiphenyl over Pd /TiO_2(B) nanosheets. *Applied Catal. B: Environ*. **2021,** *298*, 120526.

(15) Zahran, E. M.; Bedford, N. M.; Nguyen, M. A.; Chang, Y. J.; Guiton, B. S.; Naik, R. R.; Bachas, L. G.; Knecht, M. R.; Light-Activated Tandem Catalysis Driven by Multicomponent Nanomaterials, J. Am. Chem. Soc. **2014**, 136, 32-35.

(16) Li, L.; Chang, W.; Wang, Y.; Ji, H.; Chen, C.; Ma, W.; Zhao, J.; Rapid, photocatalytic, and deep debromination of polybrominated diphenyl ethers on Pd-TiO_2: intermediates and pathways, Chem. Eur. J. **2014**, 20, 11163–11170.